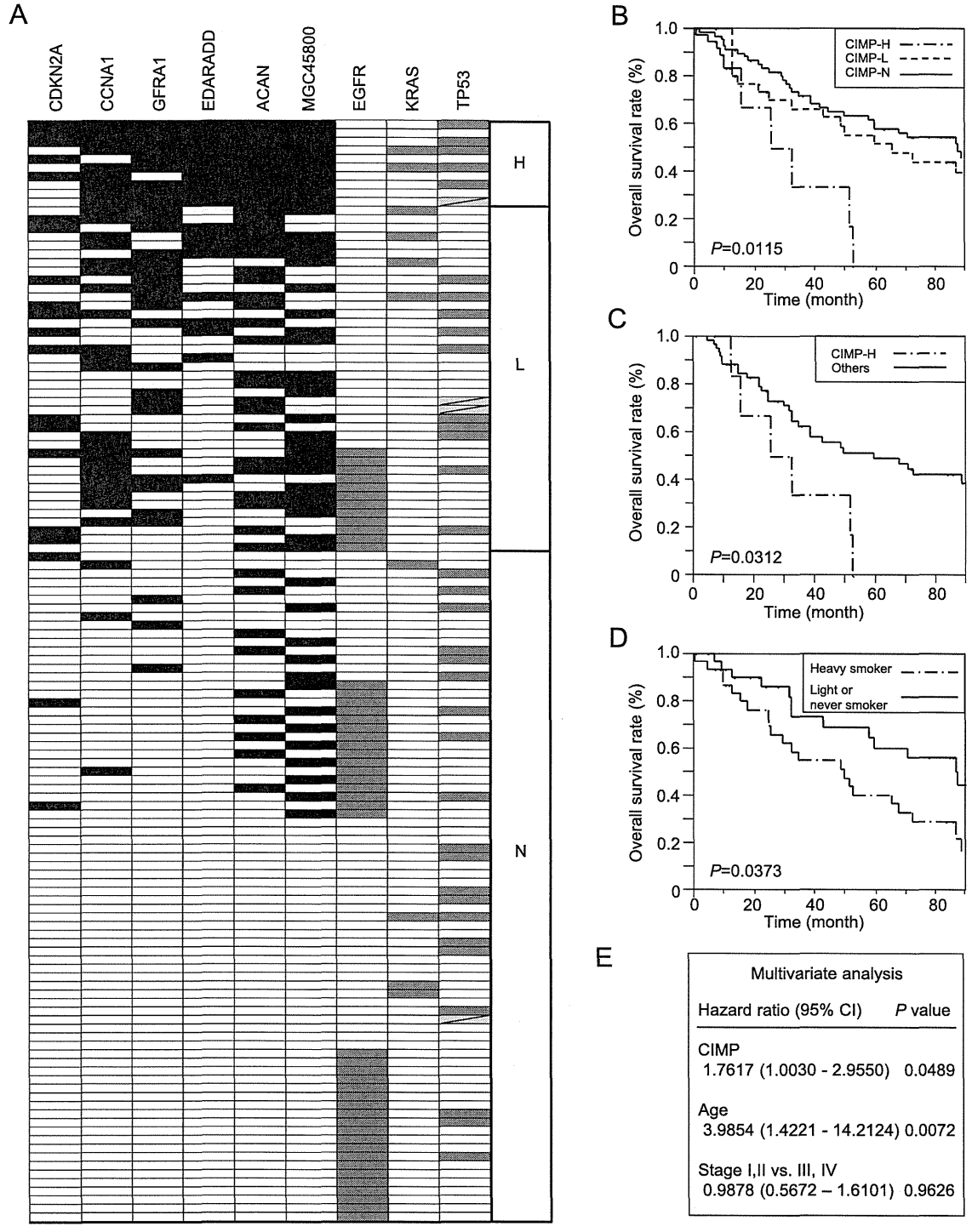

Fig. 3. CIMP status associated with prognosis of AdCas. (**A**) Total of 128 AdCas were classified into three subclasses by the six newly identified CIMP markers. Black boxes, methylation positive; gray boxes, mutation positive; white boxes, methylation negative or mutation negative and light gray boxes with oblique lines, data were not available for *TP53* status. H, CIMP-H; L, CIMP-L and N, CIMP-N. (**B**) Kaplan–Meier analysis for overall survival of 128 AdCa patients by CIMP status. *P* value was calculated by log-rank analysis. (**C**) Kaplan–Meier analysis for overall survival of 80 AdCas cases harboring wild-type *EGFR* by CIMP status. (**D**) Kaplan–Meier analysis for overall survival by smoking status. (**E**) Multivariate analysis showed that CIMP-H was an independent prognostic factor among male smokers (n = 37).

the methylation status of these 19 genes, we found that AdCas in our training set were divided into three clusters; the three most extensively methylated AdCas were consistent with the CIMP-H AdCas, suggesting that a panel of 19 genes may also be a potent predictor for CIMP-H in AdCas (Supplementary Figure 3, available at *Carcinogenesis* Online). However, given the worse prognosis of patients with CIMP-H AdCas, the impact of CIMP to survival in lung cancer might be different from the CIMP in colon cancer, glioma and breast cancer. Indeed, a study in myelodysplastic syndromes also showed that the presence of CIMP was significantly associated with poor prognosis and risk of leukemia transformation (38). The contrasting impacts of CIMP to clinical outcome might be due to the distinct DNA methylation profiles specific to each tumor type; CIMP confers poor prognosis in lung AdCas and myelodysplastic syndromes via inactivation

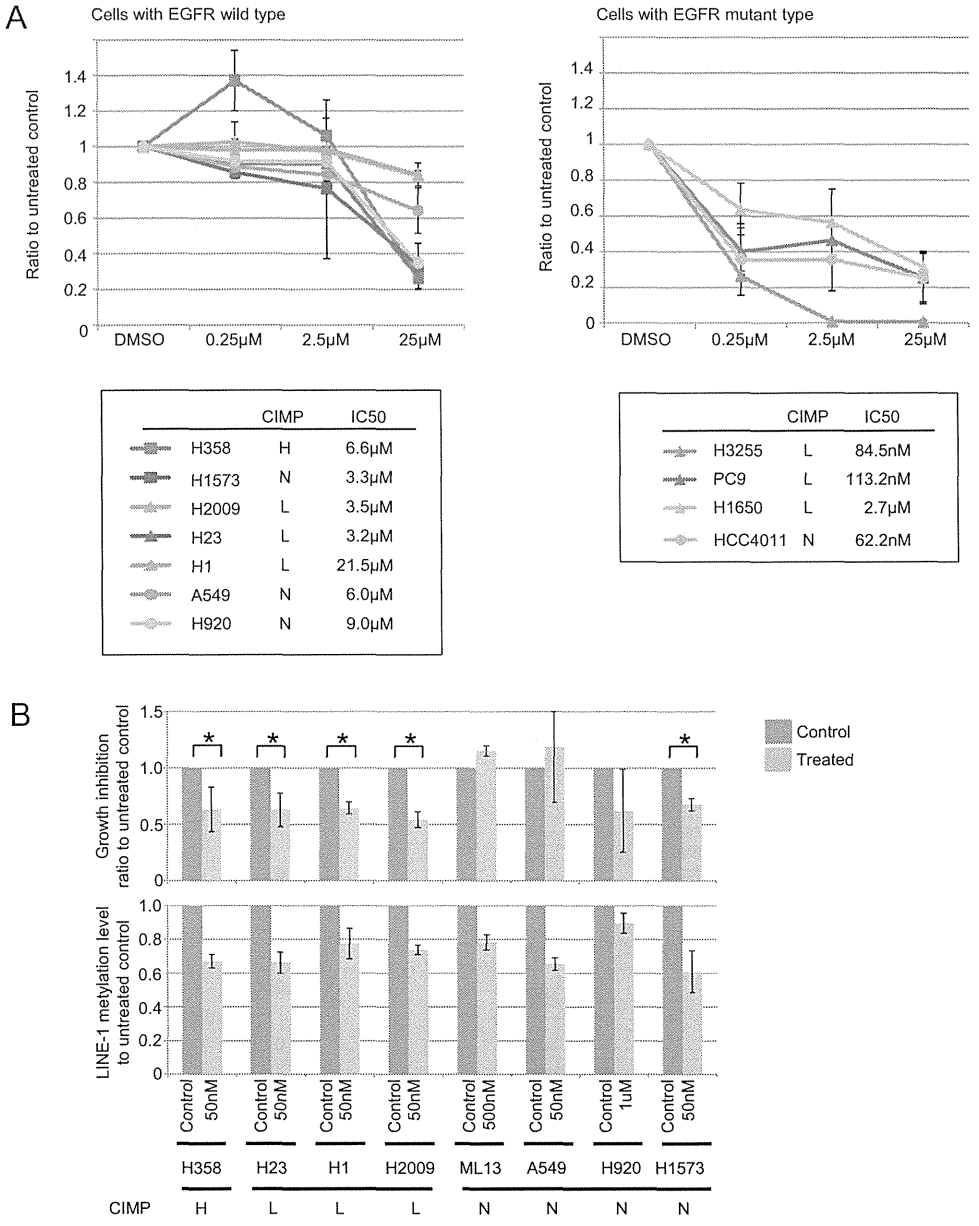

Fig. 4. Epigenetic treatment in AdCa cell lines. (**A**) Growth rate of AdCa cell lines with each *EGFR* status as measured by 3-(4,5-dimethylthiazole-2-yl)-2,5-bdiphenyl tetrazolium bromide assay after 72 h of treatment of TKI (AG1478) in different doses. CIMP status of each cell line is indicated by H, L and N. (**B**) Growth inhibition of AdCas after 5-Aza-dC treatment. Growth inhibition was examined (upper panel) at the concentration where 20% of LINE-1 demethylation had occurred (lower panel). $^{*}P < 0.05$.

of genes critical for tumor progression and for response to chemotherapy.

We found another epigenomic subgroup (CIMP-L) of AdCas within the major subclasses classified by DNA methylation status. This subtype showed moderate accumulation of DNA methylation. Indeed, our cell line study showed that CIMP-L cells were sensitive to 5-Aza-dC treatment. These data suggest that tumorigenesis pathway of CIMP-L AdCas might also be affected by DNA methylation to a certain extent. However, we could not find any specific features of this subtype. This might be due to the lack of suitable markers to further classify CIMP-L, resulting in a mixture of subpopulations as was found in the colon cancer study (39,40). Sensitive and specific markers for CIMP-L in AdCas are needed to further characterize CIMP-L. Additional studies will be required to address this problem.

CIMP-positive lung AdCa cell lines appeared to be more sensitive to 5-Aza-dC treatment, in which demethylation effectively occurred even at low doses of 5-Aza-dC, regardless of *EGFR* mutation status. Epigenetic drugs targeting DNA methylation, such as 5-Aza-dC and 5-azacytidine, have shown clinical effectiveness in cancer treatment, especially for hematological malignancies (41,42). For the treatment of thoracic malignancies, studies showed that a certain population of patients with AdCas clinically benefit from 5-Aza-dC treatment (43,44). One of the important issues of research is the identification of biomarkers predictive of response to DNA methylation inhibitors (45). Our cell line analysis showed that CIMP status appeared to be associated with response to 5-Aza-dC, suggesting that epigenetic therapy might be a useful approach, especially for those individuals who have been diagnosed with CIMP. If this possibility was validated, our findings would be significant for the use of DNA methylation inhibitors in lung tumors.

In conclusion, we demonstrated here that six newly identified CIMP markers may be useful in the accurate and practical epigenomic

classifications of lung cancer. Our findings may enable the development of new molecular diagnostics tools for personalized medicine for lung cancers and confer a new paradigm for cancer treatment.

Supplementary material

Supplementary Figures 1–3 and Tables 1–4 can be found at http://carcin.oxfordjournals.org/.

Funding

This work is supported by grants-in-aid for Cancer Research from the Ministry of Health. Labor and Welfare (to Y.K.) and a grant from the Japan Society for the Promotion of Science (to Y.K.).

Conflict of Interest Statement: None declared.

References

1. Jemal,A. *et al.* (2010) Cancer statistics, 2010. *CA Cancer J. Clin.*, **60**, 277–300.
2. Mitsudomi,T. *et al.* (2010) Gefitinib versus cisplatin plus docetaxel in patients with non-small-cell lung cancer harbouring mutations of the epidermal growth factor receptor (WJTOG3405): an open label, randomised phase 3 trial. *Lancet Oncol.*, **11**, 121–128.
3. Choi,Y.L. *et al.* (2010) EML4-ALK mutations in lung cancer that confer resistance to ALK inhibitors. *N. Engl. J. Med.*, **363**, 1734–1739.
4. Belinsky,S.A. (2004) Gene-promoter hypermethylation as a biomarker in lung cancer. *Nat. Rev. Cancer*, **4**, 707–717.
5. Jones,P.A. *et al.* (2002) The fundamental role of epigenetic events in cancer. *Nat. Rev. Genet.*, **3**, 415–428.
6. Jones,P.A. *et al.* (2007) The epigenomics of cancer. *Cell*, **128**, 683–692.
7. Toyota,M. *et al.* (1999) CpG island methylator phenotype in colorectal cancer. *Proc. Natl Acad. Sci. USA*, **96**, 8681–8686.
8. Grady,W.M. (2007) CIMP and colon cancer gets more complicated. *Gut*, **56**, 1498–1500.
9. Suzuki,M. *et al.* (2006) Exclusive mutation in epidermal growth factor receptor gene, HER-2, and KRAS, and synchronous methylation of non-small cell lung cancer. *Cancer*, **106**, 2200–2207.
10. Marsit,C.J. *et al.* (2006) Examination of a CpG island methylator phenotype and implications of methylation profiles in solid tumors. *Cancer Res.*, **66**, 10621–10629.
11. Liu,Z. *et al.* (2008) CpG island methylator phenotype involving tumor suppressor genes located on chromosome 3p in non-small cell lung cancer. *Lung Cancer*, **62**, 15–22.
12. Suzuki,M. *et al.* (2010) Molecular characterization of chronic obstructive pulmonary disease-related non-small cell lung cancer through aberrant methylation and alterations of EGFR signaling. *Ann. Surg. Oncol.*, **17**, 878–888.
13. Zhang,Y. *et al.* (2011) Methylation of multiple genes as a candidate biomarker in non-small cell lung cancer. *Cancer Lett.*, **303**, 21–28.
14. Weisenberger,D.J. *et al.* (2006) CpG island methylator phenotype underlies sporadic microsatellite instability and is tightly associated with BRAF mutation in colorectal cancer. *Nat. Genet.*, **38**, 787–793.
15. Ogino,S. *et al.* (2006) CpG island methylator phenotype-low (CIMP-low) in colorectal cancer: possible associations with male sex and KRAS mutations. *J. Mol. Diagn.*, **8**, 582–588.
16. Shen,L. *et al.* (2007) Integrated genetic and epigenetic analysis identifies three different subclasses of colon cancer. *Proc. Natl Acad. Sci. USA*, **104**, 18654–18659.
17. Gao,W. *et al.* (2008) Variable DNA methylation patterns associated with progression of disease in hepatocellular carcinomas. *Carcinogenesis*, **29**, 1901–1910.
18. Goto,Y. *et al.* (2009) Epigenetic profiles distinguish malignant pleural mesothelioma from lung adenocarcinoma. *Cancer Res.*, **69**, 9073–9082.
19. An,B. *et al.* (2010) A characteristic methylation profile in CpG island methylator phenotype-negative distal colorectal cancers. *Int. J. Cancer*, **127**, 2095–2105.
20. Okamoto,Y. *et al.* (2012) Aberrant DNA methylation associated with aggressiveness of gastrointestinal stromal tumour. *Gut*, **61**, 392–401.
21. Yang,A.S. *et al.* (2004) A simple method for estimating global DNA methylation using bisulfite PCR of repetitive DNA elements. *Nucleic Acids Res.*, **32**, e38.
22. Kondo,Y. *et al.* (2007) Alterations of DNA methylation and histone modifications contribute to gene silencing in hepatocellular carcinomas. *Hepatol Res.*, **37**, 974–983.
23. Eisen,M.B. *et al.* (1998) Cluster analysis and display of genome-wide expression patterns. *Proc. Natl Acad. Sci. USA*, **95**, 14863–14868.
24. Cover,T. *et al.* (1967) Nearest neighbor pattern classification. *IEEE Trans. Inform. Theory*, **13**, 21–27.
25. Yokoyama,T. *et al.* (2006) EGFR point mutation in non-small cell lung cancer is occasionally accompanied by a second mutation or amplification. *Cancer Sci.*, **97**, 753–759.
26. Ogino,S. *et al.* (2005) Sensitive sequencing method for KRAS mutation detection by pyrosequencing. *J. Mol. Diagn.*, **7**, 413–421.
27. Spittle,C. *et al.* (2007) Application of a BRAF pyrosequencing assay for mutation detection and copy number analysis in malignant melanoma. *J. Mol. Diagn.*, **9**, 464–471.
28. Monti,S. *et al.* (2003) Consensus clustering: a resampling-based method for class discovery and visualization of gene expression microarray data. *Mach. Learn.*, **52**, 91–118.
29. Toyota,M. *et al.* (2000) Distinct genetic profiles in colorectal tumors with or without the CpG island methylator phenotype. *Proc. Natl Acad. Sci. USA*, **97**, 710–715.
30. Noushmehr,H. *et al.* (2010) Identification of a CpG island methylator phenotype that defines a distinct subgroup of glioma. *Cancer Cell*, **17**, 510–522.
31. Fang,F. *et al.* (2011) Breast cancer methylomes establish an epigenomic foundation for metastasis. *Sci. Transl. Med.*, **3**, 75ra25.
32. Issa,J.P. (2004) CpG island methylator phenotype in cancer. *Nat. Rev. Cancer*, **4**, 988–993.
33. Lu,K.H. *et al.* (2004) Selection of potential markers for epithelial ovarian cancer with gene expression arrays and recursive descent partition analysis. *Clin. Cancer Res.*, **10**, 3291–3300.
34. Eberhard,D.A. *et al.* (2005) Mutations in the epidermal growth factor receptor and in KRAS are predictive and prognostic indicators in patients with non-small-cell lung cancer treated with chemotherapy alone and in combination with erlotinib. *J. Clin. Oncol.*, **23**, 5900–5909.
35. Toyooka,S. *et al.* (2006) Mutational and epigenetic evidence for independent pathways for lung adenocarcinomas arising in smokers and never smokers. *Cancer Res.*, **66**, 1371–1375.
36. Samowitz,W.S. *et al.* (2006) Association of smoking, CpG island methylator phenotype, and V600E BRAF mutations in colon cancer. *J. Natl Cancer Inst.*, **98**, 1731–1738.
37. Limsui,D. *et al.* (2010) Cigarette smoking and colorectal cancer risk by molecularly defined subtypes. *J. Natl Cancer Inst.*, **102**, 1012–1022.
38. Shen,L. *et al.* (2010) DNA methylation predicts survival and response to therapy in patients with myelodysplastic syndromes. *J. Clin. Oncol.*, **28**, 605–613.
39. Ogino,S. *et al.* (2008) Molecular classification and correlates in colorectal cancer. *J. Mol. Diagn.*, **10**, 13–27.
40. Yagi,K. *et al.* (2010) Three DNA methylation epigenotypes in human colorectal cancer. *Clin. Cancer Res.*, **16**, 21–33.
41. Silverman,L.R. *et al.* (2002) Randomized controlled trial of azacitidine in patients with the myelodysplastic syndrome: a study of the cancer and leukemia group B. *J. Clin. Oncol.*, **20**, 2429–2440.
42. Kantarjian,H. *et al.* (2006) Decitabine improves patient outcomes in myelodysplastic syndromes: results of a phase III randomized study. *Cancer*, **106**, 1794–1803.
43. Schrump,D.S. *et al.* (2006) Phase I study of decitabine-mediated gene expression in patients with cancers involving the lungs, esophagus, or pleura. *Clin. Cancer Res.*, **12**, 5777–5785.
44. Momparler,R.L. *et al.* (2001) Potential of 5-aza-2'-deoxycytidine (Decitabine) a potent inhibitor of DNA methylation for therapy of advanced non-small cell lung cancer. *Lung Cancer*, **34** (suppl. 4), S111–S115.
45. Garcia-Manero,G. (2010) Prognosis of myelodysplastic syndromes. *Hematology Am. Soc. Hematol. Educ. Program*, **2010**, 330–337.

Received November 20, 2011; revised April 9, 2012; accepted April 18, 2012

Malignant Pleural Mesothelioma Localized in the Thoracic Wall

Daisaku Morimoto, MD, Nobukazu Fujimoto, MD, PhD,* Hideyuki Nishi, MD, PhD,† Michiko Asano, MD,* Yasuko Fuchimoto, MD, PhD,* Katsuichiro Ono, MD,* Shinji Ozaki, MD,* Koji Taguchi, MD, PhD‡ and Takumi Kishimoto, MD, PhD*

Malignant pleural mesothelioma (MPM) usually shows a diffuse pattern of growth over the pleural surfaces. We present an unusual case of MPM that was localized and had spread outside the thoracic wall.

CASE REPORT

A 65-year-old man was referred to our hospital because of dry cough. He was a never smoker and worked at a chemical fiber factory where he was exposed to asbestos for 40 years. Physical examination revealed that the skin over the left subclavian area was swollen but without tenderness or redness.

A chest radiograph showed hypolucency on the left side. A computed tomographic scan of the chest showed a 7-cm diameter tumor on the left anterior chest wall surrounding the second rib (Fig. 1). No pleural plaque, effusion, or lymphadenopathy was detected. Fluorodeoxyglucose positron emission tomographic computed tomographic imaging showed the accumulation of fluorodeoxyglucose in the tumor with the maximum standardized uptake value of 15.1 without accumulation in any other organ. The diagnosis of MPM, epithelioid type, was made from a percutaneous needle-biopsy specimen. Thoracoscopic exploration showed that the tumor was covered with parietal pleura, and no dissemination was found on the pleura. The tumor and the involved first, second, and the third ribs were removed with curative intent. The resected specimen revealed cubiform tumor cells; some of which were forming a papillary tubular structure (Fig. 2*A*). Immunohistochemical analyses demonstrated that the tumor cells were positive for calretinin (Fig. 2*B*), D2–40, Wilms' tumor 1, thrombomodulin, cytokeratin 5/6, and epithelial membrane antigen, and negative for carcinoembryonic antigen (Fig. 2C), thyroid transcription factor, and napsin A. The diagnosis was confirmed as epithelioid type MPM. Detailed investigation of the specimen showed that the parietal pleura was involved with tumor cells (Fig. 3), indicating that the tumor originated from the parietal pleura. Six months later, he had a local recurrence and underwent radiotherapy and systemic chemotherapy.

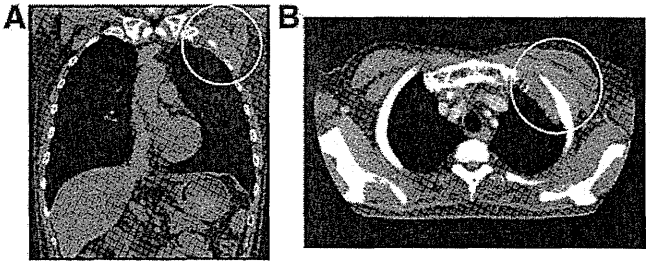

FIGURE 1. Computed tomographic scan of the chest at the time of diagnosis showing (*A*) coronal and (*B*) horizontal views of a tumor on the left anterior chest wall.

DISCUSSION

In the current case, a patient presented with MPM that localized and spread outside the thoracic wall. The tumor was initially suspected to be a soft-tissue neoplasm, osteoblastic metastatic tumor, or malignant lymphoma. The pathological diagnosis of MPM was determined from a percutaneous needle-biopsy specimen. Thoracoscopic exploration showed that the tumor was covered with parietal pleura without dissemination into the pleura, an unusual pattern of MPM progression.

MPM is classified in diffuse MPM or localized (LMPM). LMPM is uncommon and characterized by a sharply circumscribed tumor of the seromal membranes with the microscopic appearance of diffuse malignant mesothelioma, but without any evidence of diffuse spread.[1] It was formerly considered a benign variant of mesothelioma,[2] solitary fibrous tumor,[3] or other neoplasms, but is now defined as having the microscopic, histochemical, immunohistochemical, and ultrastructural features of diffuse MPM. However, little is known about the frequency and clinical behavior of LMPM.

The tumor in the current case was grossly localized in the thoracic wall. Detailed pathological analyses showed that the parietal pleura were involved with tumor cells, but diffuse pleural spread was not determined; therefore, we regard

Departments of *Respiratory Medicine, †Surgery, and ‡Pathology, Okayama Rosai Hospital, Okayama Japan.

Disclosure: The authors declare no conflict of interest.

This research is a part of the research and development and dissemination projects related to the 13 fields of occupational injuries and illnesses of the Japan Labour Health and Welfare Organization.

Address for correspondence: Nobukazu Fujimoto, MD, PhD, Department of Respiratory Medicine, Okayama Rosai Hospital, 1-10-25 Chikkomidorimachi, Minamiku, Okayama 7028055, Japan. E-mail: nfuji@okayamaH.rofuku.go.jp

ISSN: 1556-0864/12/0710-e21

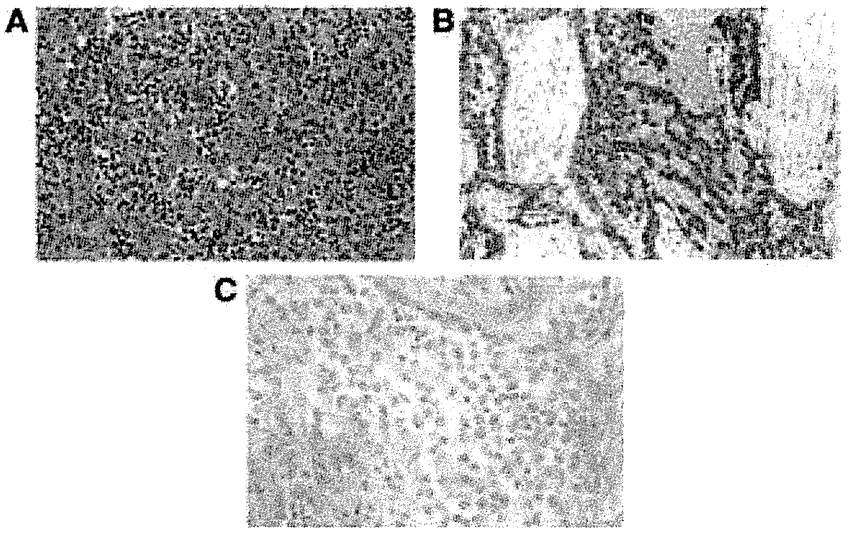

FIGURE 2. *A*, Microscopic examination of the biopsy specimen showed cubiform tumor cells; some of the cells formed papillary tubular structures consistent with malignant mesothelioma (hematoxylin-eosin, 40 ×). *B*, Immunohistochemical analysis indicated positive expression of calretinin (40 ×) and (*C*) negative expression of carcinoembryonic antigen (40 ×).

FIGURE 3. Microscopic examination of the biopsy specimen showed that the parietal pleural was involved with tumor cell (arrows), indicating that the tumor originated from the parietal pleura.

the current case as LMPM. LMPM should be considered a thoracic tumor that is localized and has spread outside the thoracic wall.

REFERENCES

1. Allen TC, Cagle PT, Churg AM, et al. Localized malignant mesothelioma. *Am J Surg Pathol* 2005;29:866–873.
2. Robinson LA Reilly RB. Localized pleural mesothelioma. The clinical spectrum. *Chest* 1994;106:1611–1615.
3. Crotty TB, Myers JL, Katzenstein AL, Tazelaar HD, Swensen SJ, Churg A. Localized malignant mesothelioma. A clinicopathologic and flow cytometric study. *Am J Surg Pathol* 1994;18:357–363.

ANTICANCER RESEARCH *32*: 4871-4876 (2012)

MicroRNA miR-34b/c Enhances Cellular Radiosensitivity of Malignant Pleural Mesothelioma Cells

YUHO MAKI[1], HIROAKI ASANO[1], SHINICHI TOYOOKA[1], JUNICHI SOH[1], TAKAFUMI KUBO[1], KUNIAKI KATSUI[2], TSUYOSHI UENO[1], KAZUHIKO SHIEN[1], TAKAYUKI MURAOKA[1], NORIMITSU TANAKA[1], HIROMASA YAMAMOTO[1], KAZUNORI TSUKUDA[1], TAKUMI KISHIMOTO[3], SUSUMU KANAZAWA[2] and SHINICHIRO MIYOSHI[1]

Departments of [1]Thoracic Surgery and [2]Radiology, Okayama University Hospital, Okayama, Japan; [3]Department of Internal Medicine, Okayama Rosai Hospital, Okayama, Japan

Abstract. *Background: We previously reported that epigenetic silencing of microRNA-34b/c (miR-34b/c) plays an important role in the pathogenesis of malignant pleural mesothelioma (MPM). We examined the impact of miR-34b/c restoration on the radiosensitivity of MPM cells. Materials and Methods: We established stable miR-34b/c and scramble transfectants of two MPM cell lines, H2052 and H28. We examined these transfectants by clonogenic survival assay, phosphorylated histone H2AX (γH2AX) foci assay, cell-cycle analysis, and western blotting. Results: The clonogenic survival assay revealed that miR-34b/c radiosensitized MPM cells. γH2AX foci assay showed that DNA double-strand break repair was delayed in miR-34b/c transfectants. The proportion of sub-G_1 phase cells was increased in miR-34b/c transfectants after irradiation. miR-34b/c inhibited expression of cyclin-D1, cyclin-dependent kinase 4/6, B-cell lymphoma-2 (BCL-2) and increased cleaved poly (ADP-ribose) polymerase (cPARP) and cleaved caspase-3 after irradiation. Conclusion: Our results indicate that miR-34b/c enhances radiosensitivity by promoting radiation-induced apoptosis and suggested that miR-34b/c might be a useful therapeutic molecule to enhance radiotherapy in MPM.*

Malignant pleural mesothelioma (MPM) is an aggressive neoplasm arising from the pleura. The prognosis of MPM is dismal, as neither chemotherapy nor radiotherapy remarkably improve its prognosis (1). Thus, an urgent need to understand the molecular biology of MPM exists so that new therapeutic strategies for MPM can be developed (2).

Correspondence to: Shinichi Toyooka, Department of Thoracic Surgery, Okayama University Hospital, 2-5-1 Shikata-cho, Kita-ku, Okayama 700-8558, Japan. Tel: +81 862357265, Fax: +81 862357269, e-mail: toyooka@md.okayama-u.ac.jp

Key Words: Malignant pleural mesothelioma, microRNA, miR-34b/c, radiation, radiosensitivity.

MicroRNAs (miRs) are a class of 17-22 nucleotide small non-coding RNAs (3). Among them, miR-34b/c has an upstream p53-binding site and is directly induced by p53 in response to oncogenic stress and DNA damage (4, 5). The known targets for miR-34b/c include mesenchymal epithelial transition factor (c-MET), cyclin-dependent kinase (CDK) 4/6, cyclin D1 (CCND1), cyclin E2 (CCNE2) (4), and BCL2 (6). Since miR-34b/c suppresses these targets, miR-34b/c is thought to play an important role in the p53 tumor suppressor network.

We previously reported that miR-34b/c was frequently methylated in MPM, compared with miR-34a (7). Aberrant methylation in the promoter region of miR-34b/c was present in 6 out of 6 MPM cell lines and in 40 (85.1%) out of 47 primary MPMs, whereas methylation of miR-34a was present in 2 (33.3%) out of 6 MPM cell lines and in 13 (27.7%) out of 47 primary MPMs. Interestingly, the introduction of miR-34b/c, but not p53, induced significant antitumor effects such as G_1-arrest, apoptosis, and the inhibition of migration, invasion and cell motility of MPM cells (7); these effects arose through the suppression of multiple targets of miR-34b/c, indicating the importance of miR-34b/c in MPM.

Although genetic alteration of p53 is rare in MPM (8), MPMs biologically exhibit an apparent p53-deficiency, resulting in anti-apoptosis effects and cell-cycle alterations. CCND1, one of the targets of miR-34b/c, is an important component of the core cell-cycle machinery. Recently, CCND1 was reported to be a therapeutic target for MPM (9). One study showed that the reduction of CCND1 enhances radiosensitivity of human cancer by suppressing DNA double-strand break (DSB) repair (10). Another report described that flavopiridol, a pan-CDK inhibitor, also enhances radiosensitivity and induces apoptosis in non-small cell lung cancer (11), as well as gastric and colon cancer (12).

After considering these points, we hypothesized that the introduction of miR-34b/c might restore p53-mediated tumor suppression in response to ionizing radiation (IR) in MPM

cells. In this study, we examined the impact of miR-34b/c on the cellular radiosensitivity of MPM cells.

Materials and Methods

Cell culture and establishment of stable miR-34b/c transfectants. Two MPM cell lines (H2052 and H28) in which the expressions of miR-34b and miR-34c were epigenetically suppressed were used in this study. The two MPM cell lines were kindly provided by Dr. Adi F. Gazdar (Department of Pathology, University of Texas Southwestern Medical Center, Dallas, TX, USA) and were maintained in RPMI-1640 (Sigma Chemical Co., Saint Louis, MO, USA) supplemented with 10% fetal bovine serum in 5% CO_2. Stable miR-34b/c and scramble RNA transfectants were established, as previously described in our report (7). Briefly, a fragment of genomic DNA encoding miR-34b/c or scramble RNA fragment as a negative control was subcloned into a pSilencer 4.1-CMV neo plasmid vector (Ambion, Austin, TX, USA). The constructed plasmids were then transfected into MPM cells using Lipofectamine 2000 Reagent (Invitrogen, Carlsbad, CA, USA). Resistant clones were isolated by G418 selection for two weeks and were maintained in G418-containing medium.

Evaluation of miR-34b/c expression using quantitative real-time-polymerase chain reaction (PCR). microRNA was extracted from miR-34b/c-transfected and scramble RNA-transfected MPM cells using TaqMan MicroRNA Cells-to-CT™ Kit (Ambion). Real-time PCR for miR-34b and 34c was performed using TaqMan MicroRNA Assays (P/N4427975, Assay ID 000427 for has-miR-34b, Assay ID 000428 for has-miR-34c; Applied Biosystems, Foster City, CA) using the StepOnePlus™ Real-Time PCR system (Applied Biosystems). The expression of miR-374 was used as an endogenous control following the manufacturer's recommendation (www.appliedbiosystems.com). The relative expression ratio for miR-34b and miR-34c was calculated from triplicate PCR.

Clonogenic cell survival assay. miR-34b/c-transfected and scramble RNA-transfected H2052 and H28 cells were trypsinized to generate a single-cell suspension, and a specified number of cells were seeded into each well in six-well tissue culture plates. After allowing the cells time to attach (6 h), the plates were irradiated at 2, 4, 6 or 8 Gy. Fourteen days after IR, colonies were stained with crystal violet. The number of colonies containing at least 50 cells was determined, and survival curves were generated. The dose enhancement factor (DEF) was calculated at a surviving fraction of 0.1 to estimate the increase in radiosensitivity. Data presented are the mean±standard deviation (SD) from at least two independent experiments.

Immunofluorescent staining for phosphorylated histone H2AX (γH2AX). γH2AX has been established as a sensitive indicator of DNA DSB with the resolution of foci corresponding to DNA DSB repair (13). miR-34b/c-transfected and scramble RNA-transfected H2052 cells were grown in Lab-Tek chamber slides (Nalge Nunc International, Naperville, IL, USA). The cells were fixed in 4% paraformaldehyde for 10 min at 1 h, 6 h, and 24 h after IR (4 Gy) and permeabilized in phosphate-buffered saline (PBS) containing 0.2% NP40 for 15 min. The cells were then incubated overnight at 4°C with 1:200 diluted anti-γH2AX antibody (Millipore, Billerica, MA,USA). The cells were incubated with 1:50 diluted fluorescein isothiocyanate (FITC)-labeled secondary antibody (Jackson Immuno Research Labs, West Grove, PA, USA) for 1 h and were then incubated in PBS, containing 4',6-diamidino-2-phenylindole (1 μg/ml) for 30 min. Coverslips were mounted using an anti-fade solution (DAKO Corp., Carpinteria, CA, USA). The slides were examined under a fluorescent microscope (Keyence BZ-8000; Keyence, Osaka, Japan). The number of γH2AX foci was counted in each nucleus, of at least 50 cells in each sample.

Cell-cycle analysis. The cell-cycle distribution was evaluated using flow cytometry in miR-34b/c-transfected and scramble RNA-transfected H2052 cells. Non-irradiated transfectants and 4 Gy-irradiated transfectants at 24 h after IR were harvested and resuspended in PBS containing 0.2% Triton X-100 and 1 mg/ml RNase, then stained with propidium iodide and analyzed using a FACScan instrument, as previously described (7). Doublets, cell debris, and fixation artifacts were gated out, and cell-cycle analysis was performed using the CellQuest version 3.1 software.

Western blot analysis. Cells were harvested and western blot analysis was carried out as previously described (7). We examined four molecules (CCND1, CDK4, CDK6, and BCL2) reported to be primary targets of miR-34b/c. We also examined BCL2 Associated X-protein (BAX), cPARP, pro-caspase-3, and cleaved caspase-3 to detect apoptosis. Actin was used as the loading control. The primary antibodies used for western blotting were as follows: anti-CCND1 (sc718, diluted 1000:1; Santa Cruz, Santa Cruz, CA, USA), anti-CDK4 (sc260, diluted 200:1; Santa Cruz), anti-CDK6 (#3136, diluted 2000:1; Cell Signaling), anti-BCL2 (sc7382, diluted 500:1; Santa Cruz), anti-BAX (#2774, diluted 1000:1; Cell Signaling Technology, Beverly, MA, USA), anti-cPARP (#9546, diluted 2000:1; Cell Signaling), anti-pro-caspase-3 (sc7272, diluted 2000:1; Santa Cruz), and anti-actin (MAB1501, diluted 20000:1; Millipore).

Statistical analysis. Data are represented as the mean±SD. An unpaired Student's *t*-test was used to compare data between the two groups. Probability values less than 0.05 were considered statistically significant. All the data were analyzed using JMP9.0 for Windows (SAS Institute, Cary, NC, USA).

Results

Evaluation of miR-34b/c expression using quantitative real-time PCR. The expressions of miR-34b and 34c were examined in miR-34b/c and scramble RNA transfectants. Compared with the scramble RNA transfectants, the expression of miR-34b was increased by 26.6-fold and 10.5-fold in miR-34b/c-transfected H2052 and H28 cells, respectively. The expression of miR-34c was increased by 68.7-fold and 31-fold in miR-34b/c-transfected H2052 and H28 cells, respectively. Compared with the increase of miR-34b and miR-34c in miR-34b/c transfectants, the expression of miR-34b and miR-34c in scramble RNA-transfected H2052 cells at 24 hours after 4 Gy IR was only increased by 1.2-fold and 1.4-fold, respectively. Thus, we confirmed that the expression of mature miR-34b and miR-34c were increased in stable miR-34b/c transfectants.

Effect of miR-34b/c on cellular radiosensitivity. A clonogenic survival assay was performed to examine the effect of miR-

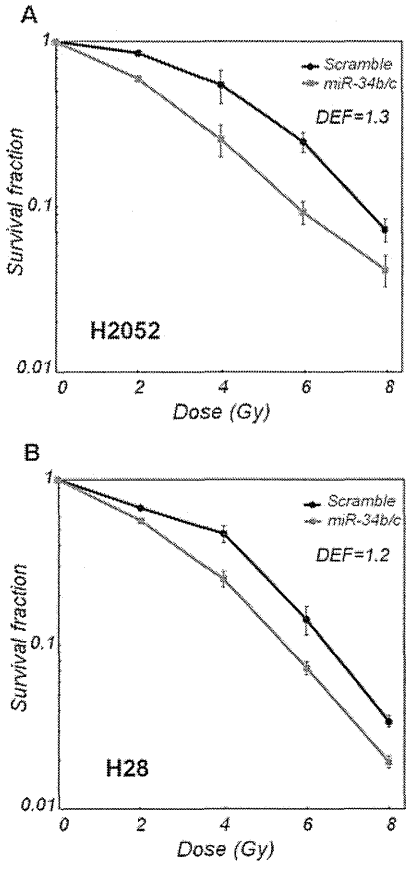

Figure 1. *Effect of miR-34b/c on cellular radiosensitivity in malignant pleural mesothelioma (MPM) cells. miR-34b/c-transfected and scramble RNA-transfected MPM cells, H2052 (A) and H28 (B), were irradiated with graded doses of X-rays. The colony-forming efficiency was determined at 14 days after irradiation, and survival curves were generated. Data are the mean±SD of two independent experiments. DEF, Dose-enhancement factor.*

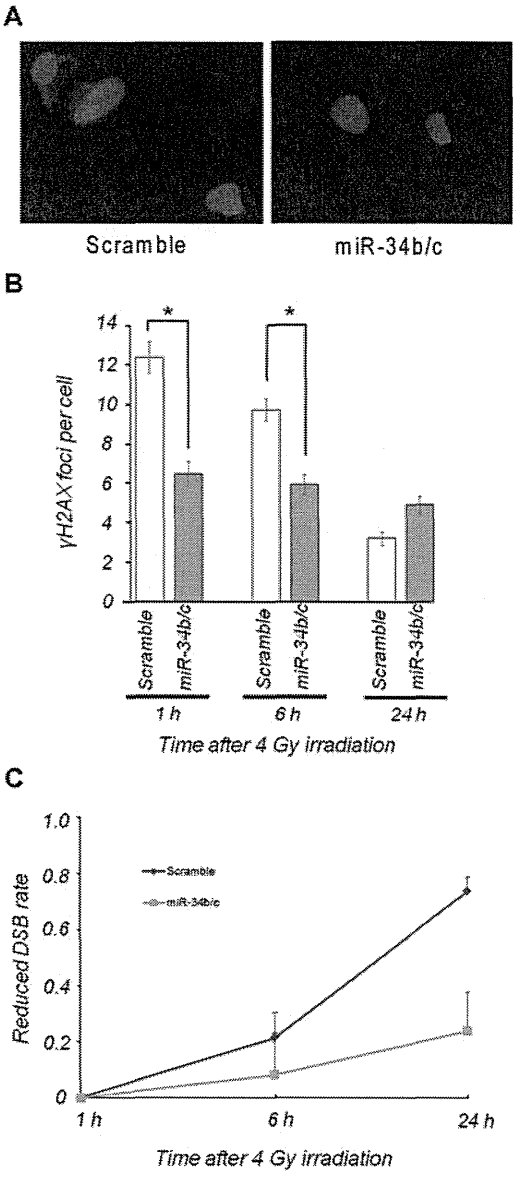

Figure 2. *Effect of miR-34b/c on radiation-induced phosphorylated histone H2AX (γH2AX) foci in H2052 cells. A: Representative micrographs obtained from scramble RNA-transfected H2052 cells (left) and miR-34b/c-transfected H2052 cells (right) at 1 h after irradiation (4 Gy). B: miR-34b/c-transfected and scramble RNA-transfected H2052 cells on growing chamber slides were exposed to irradiation (4 Gy) and fixed at a specific time for use in immunocytochemical analyses of the nuclear γH2AX foci. Foci were evaluated in 50 nuclei per treatment for each sample. Data are the mean±SEM. *p<0.05. C: Reduced double-strand break (DSB) rate in miR-34b/c-transfected and scramble RNA-transfected H2052 cells at 1, 6 and 24 h after 4 Gy irradiation. Data are the mean+SEM of two independent experiments.*

34b/c on radiosensitivity in miR-34b/c transfectants, compared with the scramble control. As shown in Figure 1, miR-34b/c enhanced radiosensitivity of both miR-34b/c-transfected H2052 and H28 cells, with a DEF of 1.3 and 1.2, respectively. Because the radiosensitizing effect of miR-34b/c was stronger in H2052 cells than that in H28 cells, subsequent experiments were performed using H2052-derived transfectants.

Effect of miR-34b/c on radiation-induced γH2AX foci. We examined the DNA damage repair potential using a γH2AX foci assay. Representative micrographs are shown in Figure 2A. Compared with the scramble RNA transfectant, the number of γH2AX foci in miR-34b/c-transfected H2052 was significantly lower at 1 and 6 hours (considered to be early-phase) after IR but was higher at 24 hours (considered to be late-phase) (Figure 2B). We also calculated the rate of reduced γH2AX foci at 6 hours and 24 hours compared with 1 hour, *i.e.* the named reduced DSB rate (NDR). The formula to calculate the NDR is as followed: (γH2AX foci per cell at 1 hour-γH2AX foci per cell at 24 hours)/γH2AX foci per

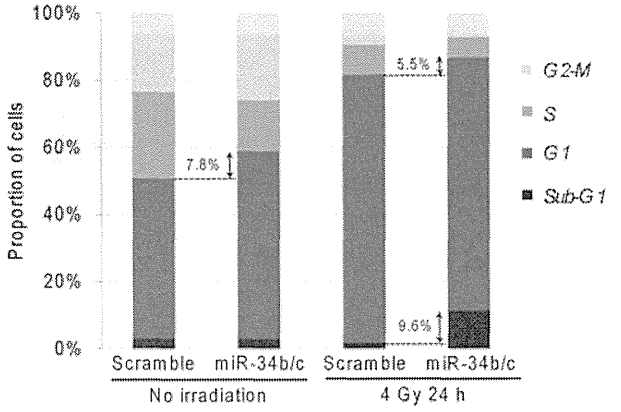

Figure 3. *Influence of miR-34b/c on the cell-cycle distribution. miR-34b/c-transfected and scramble RNA-transfected H2052 cells were irradiated at 4 Gy. The cells were collected at 24 h after irradiation. The cell-cycle distribution was determined using flow cytometry according to an analysis of propidium iodide-stained cells. Data shown are representative of two independent experiments.*

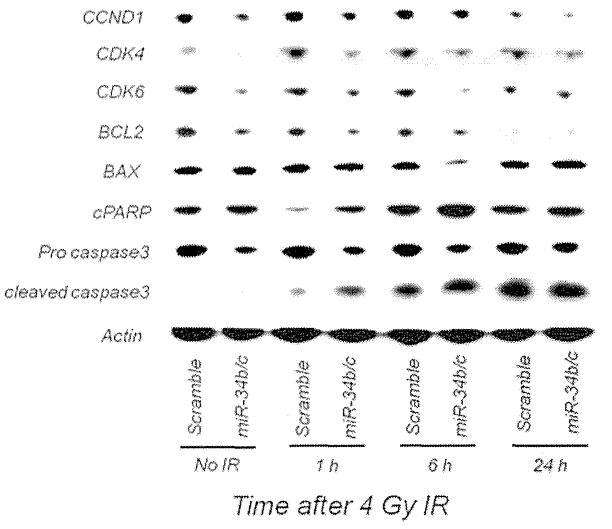

Figure 4. *Effect of miR-34b/c on primary target proteins and apoptosis-related proteins. miR-34b/c-transfected and scramble RNA-transfected H2052 cells were irradiated (4 Gy) and harvested at the specified times. The putative target proteins of miR-34b/c, namely (cyclin-D1, CCND1), cyclin dependent kinase-4 (CDK4), cyclin dependent kinase-6 (CDK6), and B-cell lymphoma-2 (BCL2) and apoptosis-related proteins BCL2 Associated X-protein (BAX), cleaved poly (ADP-ribose) polymerase (cPARP), procaspase-3, and cleaved caspase-3 were examined. Each blot is representative of two independent experiments. IR: Irradiation.*

cell at 1 hour. NDR was lower in miR-34b/c transfectants (24.0%) than that in scramble transfectants (73.8%) at 24 h after IR (Figure 2C). This result suggests that DNA DSB repair potential was impaired in miR-34b/c transfectants compared with the scramble transfectants.

miR-34b/c induced G_1 arrest and apoptosis. To further investigate the mechanism responsible for the radiosensitization effect of miR-34b/c, we performed a cell-cycle analysis on H2052 cells. The percentage of sub-G_1 and G_1 phase miR-34b/c transfectants was increased by 7.8% in non-irradiated H2052 cells and by 5.5% in 4-Gy-irradiated H2052 cells at 24 hours after IR (Figure 3). Focusing on the apoptotic fraction, the sub-G_1 phase was increased by 9.6% in miR-34b/c-transfected H2052 cells at 24 hours after IR, suggesting that miR-34b/c enhanced radiation-induced apoptosis.

Impact of miR-34b/c on primary target proteins and apoptosis-related proteins. To examine the effect of miR-34b/c on its target proteins and apoptosis-related proteins, we focused on CCND1, CDK4/6, and BCL2 as targets of miR-34b/c and BAX, cPARP, pro-caspase 3, and cleaved caspase-3 for detecting apoptosis. The expressions of CCND1, CDK4/6 and BCL2 in miR-34b/c transfected H2052 cells were down-regulated at almost all the time points after IR that were examined (Figure 4). The expression of pro-caspase-3 was decreased in miR-34b/c transfectants. In contrast, the expressions of cleaved Caspase-3 and cPARP was increased in miR-34b/c transfectants and gradually increased after IR. These results suggested that miR-34b/c suppressed its target proteins and that IR enhanced apoptosis of miR-34b/c transfectants.

Discussion

In this study, a clonogenic survival assay revealed that the restoration of miR-34b/c enhanced the radiosensitivity of MPM cells. This result is the essential finding of the present study. To understand the mechanism of radiosensitization, we focused on DNA DSB repair, cell-cycle distribution, and expression of the target proteins of miR-34b/c and apoptosis-related proteins.

Firstly, we estimated the DNA DSB status by counting γH2AX foci. The number of γH2AX foci after IR was lower at the early-phase but higher at the late-phase and the NDR was low in miR-34b/c transfectants compared with the scramble transfectants. As translation of this result, two possibilities should be considered: i) DNA DSB repair was impaired in miR-34b/c transfectants in the early-phase and DSBs accumulated at the late-phase, ii) miR-34b/c transfectants contained a low amount of DNA because miR-34b/c itself influenced the cell cycle, resulting in a low rate of cells entering the S phase. To understand how miR-34b/c impaired DNA DSB repair, CCND1, a putative target of miR-34b/c, seems to play a crucial role. Reportedly, CCND1 binds directly to RAD51 and is recruited to sites of DNA damage, and a reduction in CCND1 impairs the recruitment of RAD51 to damaged DNA and increases the cellular radiosensitivity (10). We confirmed that miR-34b/c suppresses CCND1 with

or without IR and that the suppression was greater in miR-34b/c transfectants at 24 hours after IR. Accordingly, miR-34b/c is assumed to impair DNA DSB repair by suppressing CCND1. This is considered to be a part of the mechanism by which miR-34b/c enhances radiosensitivity.

Secondly, we estimated the cell-cycle distribution and related proteins. We observed that the proportion of sub-G_1 phase miR-34b/c transfectants at 24 hours after IR was significantly greater than that for scramble transfectants, indicating that radiation-induced apoptosis took place in miR-34b/c transfectants. Of note, BCL2 expression was inhibited and that of cPARP and cleaved caspase-3 were increased in miR-34b/c transfectants after IR. As other cell-cycle-related targets of miR-34b/c, CCND1, CCNE2, CDK4 and CDK6 are known as key molecules for the G_1 checkpoint (4, 6, 14), and some of these targets were confirmed to be down-regulated in miR-34b/c transfectants in the present study. Indeed, G_1 arrest occurred in miR-34b/c transfectants. However, a question arises here. Generally cells in the G_1 phase are considered to be relatively radioresistant compared with those in other phases (15). There are several reports that explain this contradiction. Kodym *et al.* reported that flavopiridol, a pan-CDK inhibitor, was reported to increase the radiosensitivity of both proliferating and quiescent lung cancer cells by suppressing DNA DSB repair thorough a cell cycle-unrelated mechanism (11). Other studies have demonstrated CDK inhibitor-mediated G_1 arrest and radiation-induced apoptosis in breast cancer (16), as well as colonic and gastric cancer (12). We observed that miR-34b/c suppressed CDK4/6, which indicates that miR-34b/c has similar effects to a CDK inhibitor. Considering these, the effects of miR-34b/c on impairing DNA DSB repair and suppressing cell-cycle-related proteins resulted in an enhancement of radiosensitivity of MPM cells.

In conclusion, we revealed that the restoration of miR-34b/c in MPM cells enhanced radiosensitivity and promoted radiation-induced apoptosis, indicating that miR-34b/c, used in combination with IR, may be a potential therapeutic target for MPM.

Acknowledgements

We greatly acknowledge the grant support from the 13 fields of occupational injuries and illnesses of the Japan Labor Health and Welfare Organization (T. Kishimoto). We thank Mr. Seiji Tabara and Mr. Hirofumi Uno (Department of Radiology, Okayama University Hospital) for irradiating the MPM cells. We also thank Professor Adi F. Gazdar (Hammon Center for Therapeutic Oncology Research, University of Texas Southwestern Medical Center, Dallas, TX, USA) for the kind gift of cell lines.

References

1 Baas P: Chemotherapy for malignant mesothelioma. Lung Cancer *49(Suppl 1)*: S61-64, 2005.

2 Zucali PA, Ceresoli GL, De Vincenzo F, Simonelli M, Lorenzi E, Gianoncelli L and Santoro A: Advances in the biology of malignant pleural mesothelioma. Cancer Treat Rev *37*: 543-558, 2011.

3 Bentwich I: Prediction and validation of microRNAs and their targets. FEBS Lett *579*: 5904-5910, 2005.

4 He L, He X, Lim LP, de Stanchina E, Xuan Z, Liang Y, Xue W, Zender L, Magnus J, Ridzon D, Jackson AL, Linsley PS, Chen C, Lowe SW, Cleary MA and Hannon GJ A: microRNA component of the p53 tumour suppressor network. Nature *447*: 1130-1134, 2007.

5 He X, He L and Hannon GJ: The guardian's little helper: microRNAs in the p53 tumor suppressor network. Cancer Res *67*: 11099-11101, 2007.

6 He L, He X, Lowe SW and Hannon GJ: microRNAs join the p53 network – another piece in the tumour-suppression puzzle. Nat Rev Cancer *7*: 819-822, 2007.

7 Kubo T, Toyooka S, Tsukuda K, Sakaguchi M, Fukazawa T, Soh J, Asano H, Ueno T, Muraoka T, Yamamoto H, Nasu Y, Kishimoto T, Pass HI, Matsui H, Huh NH and Miyoshi S: Epigenetic silencing of microRNA-34b/c plays an important role in the pathogenesis of malignant pleural mesothelioma. Clin Cancer Res *17*: 4965-4974, 2011.

8 Toyooka S, Kishimoto T and Date H: Advances in the molecular biology of malignant mesothelioma. Acta Med Okayama *62*: 1-7, 2008.

9 Saini SS and Klein MA: Targeting cyclin D1 in non-small cell lung cancer and mesothelioma cells by antisense oligonucleotides. Anticancer Res *31*: 3683-3690, 2011.

10 Jirawatnotai S, Hu Y, Michowski W, Elias JE, Becks L, Bienvenu F, Zagozdzon A, Goswami T, Wang YE, Clark AB, Kunkel TA, van Harn T, Xia B, Correll M, Quackenbush J, Livingston DM, Gygi SP and Sicinski P: A function for cyclin D1 in DNA repair uncovered by protein interactome analyses in human cancers. Nature *474*: 230-234, 2011.

11 Kodym E, Kodym R, Reis AE, Habib AA, Story MD and Saha D: The small-molecule CDK inhibitor, SNS-032, enhances cellular radiosensitivity in quiescent and hypoxic non-small cell lung cancer cells. Lung Cancer *66*: 37-47, 2009.

12 Jung C, Motwani M, Kortmansky J, Sirotnak FM, She Y, Gonen M, Haimovitz-Friedman A and Schwartz GK: The cyclin-dependent kinase inhibitor flavopiridol potentiates gamma-irradiation-induced apoptosis in colon and gastric cancer cells. Clin Cancer Res *9*: 6052-6061, 2003.

13 Rogakou EP, Pilch DR, Orr AH, Ivanova VS and Bonner WM: DNA double-stranded breaks induce histone H2AX phosphorylation on serine 139. J Biol Chem *273*: 5858-5868, 1998.

14 Corney DC, Flesken-Nikitin A, Godwin AK, Wang W and Nikitin AY: MicroRNA-34b and MicroRNA-34c are targets of p53 and cooperate in control of cell proliferation and adhesion-independent growth. Cancer Res *67*: 8433-8438, 2007.

15 Wilson GD: Radiation and the cell cycle, revisited. Cancer Metastasis Rev *23*: 209-225 2004.

16 Carlson BA, Dubay MM, Sausville EA, Brizuela L and Worland PJ: Flavopiridol induces G_1 arrest with inhibition of cyclin-dependent kinase (CDK) 2 and CDK4 in human breast carcinoma cells. Cancer Res *56*: 2973-2978, 1996.

Received August 18, 2012
Revised October 8, 2012
Accepted October 9, 2012

医学と薬学
68巻1号・2012年7月
68(1)：177-183，2012

悪性中皮腫の血清診断における可溶性メソテリン関連ペプチド（SMRP：Soluble Mesothelin-related Peptides）の有用性に関する多施設共同試験

福岡　和也[1)]・関戸　好孝[2)]・樋田　豊明[3)]・河原　邦光[4)]
太田　三徳[5)]・松村　晃秀[6)]・岡田　守人[7)]・岸本　卓巳[8)]
中野喜久雄[9)]・中野　孝司[1)]

要　旨

悪性中皮腫の血清診断における可溶性メソテリン関連ペプチド（soluble mesothelin-related peptides：SMRP）の診断性能を多施設共同試験によって検討した。対象は，悪性中皮腫85例，比較対照疾患としての肺癌240例，良性呼吸器疾患（石綿非関連良性疾患136例，石綿関連良性疾患157例），高血圧・慢性心疾患74例および石綿曝露歴のない健常者110名。Chemiluminescent enzyme immunoassay（CLEIA）法による血清SMRP濃度測定キット（ルミパルス® メソテリン）を用いて血清SMRP濃度を測定した。参考基準値を1.5 nmol/Lに設定した場合の各対象の陽性率は，悪性中皮腫66%，肺癌21%，石綿非関連良性疾患18%，石綿関連良性疾患15%，高血圧・慢性心疾患9%，健常者1%であった。また，悪性中皮腫における血清SMRP濃度は，比較対照群および健常者に比較して有意に高値であった。原発部位別の陽性率は，胸膜65%，腹膜86%であった。悪性胸膜中皮腫の各病期におけるSMRP陽性率は，Ⅰ期（64%），Ⅱ期（67%），Ⅲ期（55%），Ⅳ期（69%）であった。また，各組織型におけるSMRP陽性率は，上皮型（65%），二相型（60%），肉腫型（75%），であった。今回のルミパルス® メソテリンを用いた試験結果では，悪性中皮腫の血清診断におけるSMRPの診断性能は，これまでの報告と同等であった。さらに，悪性胸膜中皮腫早期例，肉腫型および腹膜中皮腫における診断的有用性も示唆された。

1）兵庫医科大学内科学呼吸器RCU科　2）愛知県がんセンター研究所分子腫瘍学部　3）同　中央病院呼吸器内科　4）大阪府立病院機構大阪府立呼吸器アレルギー医療センター病理診断科　5）同　呼吸器外科　6）国立病院機構近畿中央胸部疾患センター呼吸器外科　7）広島大学医学部腫瘍外科　8）労働者健康福祉機構岡山労災病院内科　9）国立病院機構呉医療センター呼吸器内科

Evaluation of the usefulness of SMRP (Soluble Mesothelin-related Peptides) for the diagnosis of malignant mesothelioma

Kazuya Fukuoka, Takashi Nakano et al　*Division of Respiratory Medicine, Department of Internal Medicine, Hyogo College of Medicine*

Key words：malignant mesothelioma（悪性中皮腫），SMRP，soluble mesothelin-related peptides（可溶性メソテリン関連ペプチド），biomarker（バイオマーカー），early detection of mesothelioma（悪性中皮腫の早期診断）

はじめに

悪性中皮腫（malignant mesothelioma，MM）は体腔内面を広く覆う漿膜に発生する腫瘍で，胸膜，腹膜，心膜，および非常にまれではあるが，精巣鞘膜からも発生する。この中で，胸膜由来の悪性胸膜中皮腫（malignant pleural mesothelioma：MPM）が最も多い。これまで，MMは非常にまれな疾患とされてきたが，本疾患と石綿曝露との密接な関連性が報告されてから半世紀が経過した現在，その罹患者数および死亡者数は世界的に急激な増加を辿っている[1)2)]。MPMの予後は不良であり，生存期間中央値は9～17カ月とされている[3)]。MPMの早期発見は非常に困難であり，確定診断が得られた時点では，すでに進行期である症例が大多数を占める。MPMに対する標準的治療法はいまだに確立されておらず，手術療法によって腫瘍が肉眼的に完全切除されても治癒に至る症例は極めて少ない。したがって，治療成績の向上には，疾患の早期発見と手術療法に化学療法や放射線療法などを組み合わせた集学的治療を確立することが極めて重要な役割を果たす[4)]。

MPMの早期診断には，画像検査や胸腔鏡検査の進歩とともに，血清や体腔液診断に有用なバイオマーカーの開発が必要不可欠である。現在，MPMの血清診断における新規バイオマーカーとして最も注目されている分子が，可溶性メソテリン関連ペプチド（soluble mesothelin-related peptides：SMRP）である[5)]。SMRP本体の蛋白であるメソテリンは，膵臓癌，卵巣癌，中皮腫やその他の癌に過剰発現する40 kDaの細胞膜表面に存在する糖蛋白である。メソテリンは癌特異的抗原ではなく，胸膜，腹膜および心膜の正常中皮細胞にも発現する分化抗原と考えられている。メソテリンの遺伝子は69 kDaの前駆蛋白（mesothelin/megakaryocyte potentiating factor：MPF family proteins）をコードし，この糖蛋白はfurin-like proteinaseで切断後N末端側は31 kDaのMPFとして血中に放出される。C末端側40 kDaの糖蛋白はメソテリンとして細胞膜に結合している。メソテリンには3種類のvariant formが知られおり，そのうちのひとつは修飾されたカルボキシル基終末をもち，GPIアンカーを欠如するために細胞膜から遊離する。このsoluble isoformがSMRPに相当するとされる[6)]。2003年，Robinsonらは血清SMRPのMPMにおける診断的意義に関する最初の報告を行った[7)]。近年，SMRPを認識する2種類のモノクローナル抗体（OV569と4H3）を用いた新しい定量的enzyme-linked immunosorbent assay（ELISA）キットであるMESOMARK™の開発によって，血清SMRP濃度の測定が可能となった。このキットを用いて，SMRPのMMに対する診断性能を検討した研究が欧米や豪州から報告されている[8)～16)]。

今回，われわれは，MESOMARK™と同一の抗体を用いたchemiluminescent enzyme immunoassay（CLEIA）法による血清SMRP濃度測定キット（ルミパルス® メソテリン）を用いて，MM血清診断におけるSMRPの診断性能を多施設共同試験によって検討した。

Ⅰ．試験実施施設および対象

本試験は，愛知県がんセンター，大阪府立呼吸器・アレルギー医療センター，国立病院機構近畿中央胸部疾患センター，兵庫医科大学，兵庫県立成人病センター，労働者健康福祉機構岡山労災病院，国立病院機構呉医療センターの合計7施設にて，各施設の倫理委員会の審査・承認を受けて，2005年から2006年に多施設共同試験として実施した。

対象は，各施設を受診したMM患者および対照疾患患者のうち，試験参加に関して文書で同意が得られた被験者および健常者（石綿曝露歴のない院内ボランティア）の計802例である。MM85例のうち，MPMは77例で，7例が悪性腹膜中皮腫，1例が精巣鞘膜由来の中皮腫であった。比較対照疾患の内訳は，肺癌，良性呼吸器疾患（石綿非関連良性疾患および石綿関連良性疾患），石綿曝露歴のない高血圧・慢性心疾

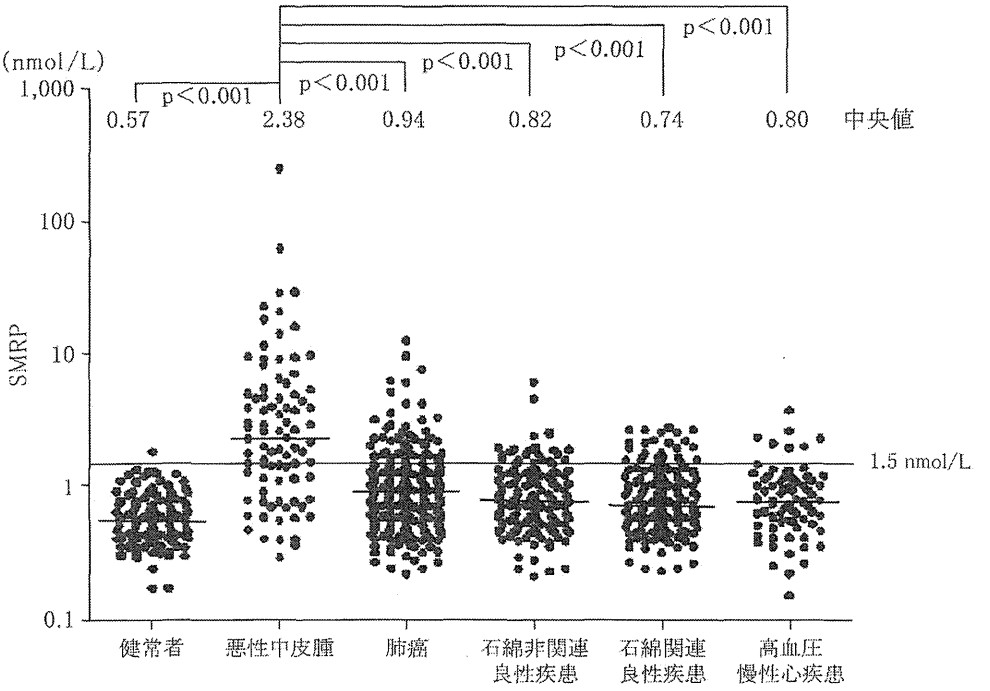

図 1　悪性中皮腫および対照疾患における血清 SMRP 濃度の分布

表 1　悪性中皮腫および対照疾患における血清 SMRP 濃度および陽性率

	健常者	悪性中皮腫	肺癌	石綿非関連良性疾患	石綿関連良性疾患	高血圧・慢性心疾患
症例総数	110	85	240	136	157	74
中央値（nmol/L）	0.57	2.38	0.94	0.82	0.74	0.80
SD（nmol/L）	0.30	28.57	1.36	0.74	0.58	0.62
陽性数	1	56	51	24	24	7
陽性率	1%	66%	21%	18%	15%	9%

SD：standard deviation

患であった（**表 1**）。

II. 血清 SMRP 濃度の測定

すべての被験者に対して採血を実施し，速やかに血清を分離後，−80℃にて凍結保存した。

血清 SMRP 濃度は，体外診断用医薬品として 2010 年 10 月に認可されたルミパルス® メソテリン（富士レビオ株式会社製造）を用いて測定した。本キットは，米国，カナダ，ヨーロッパおよびオーストラリア等で販売されている ELISA 法による SMRP 測定キットである MESOMARK™ と同一の抗体を用いた，2 ステップサンドイッチ法に基づく CLEIA 法による SMRP 測定試薬である。本試薬は，全自動化学発光酵素免疫測定システム用試薬であり，約 30 分間で測定が完了し，測定範囲は 0.1 から 100 nmol/L に及ぶ。MESOMARK™ との相関性は，ほぼ 1：1 であり，同等の測定結果の得られることが報告されており，参考基準値は両者ともに 1.5 nmol/L に設定されている[9)17)]。

統計学的解析には，statistical package for social science（SPSS）を使用し，2 群間の有意

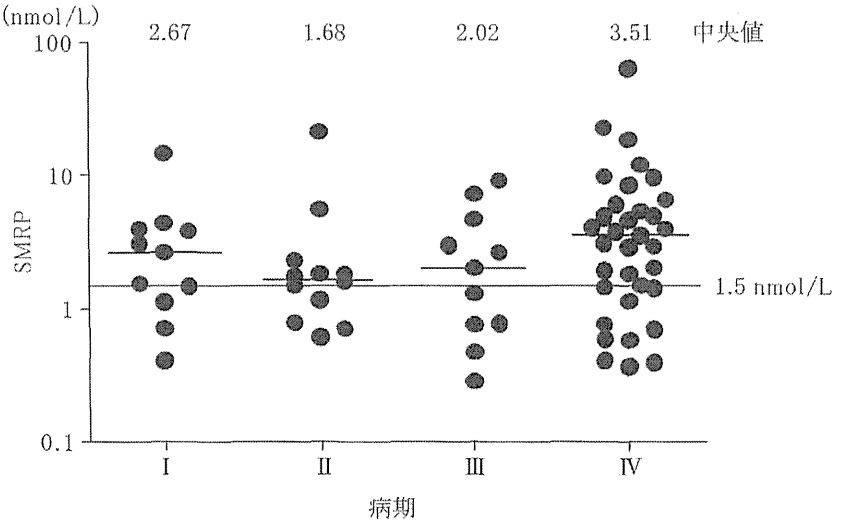

図 2　悪性胸膜中皮腫の各病期における血清 SMRP 濃度の分布

表 2　悪性胸膜中皮腫の各病期における血清 SMRP 濃度および陽性率

	I	II	III	IV
症例総数	11	12	11	35
中央値（nmol/L）	2.67	1.68	2.02	3.51
SD（nmol/L）	3.92	5.67	2.93	11.05
陽性数	7	8	6	24
陽性率	64%	67%	55%	69%

SD：standard deviation

差検定は Mann-Whitney 検定を用いて行った。各図中には測定値の中央値を示した（単位は nmol/L）。

III. 結　　果

1．健常者における血清 SMRP 濃度

石綿曝露歴のない健常者 110 例の血清 SMRP 濃度を測定し，測定結果を対数変換した結果，SMRP 測定値の正規分布が確認された。SMRP 測定値は，1 例（1.86 nmol/L）を除き，すべて参考基準値（1.5 nmol/L）未満であった（陰性率 99.1%）。

2．MM および比較対照疾患における血清 SMRP 濃度および陽性率（図 1，表 1）

血清 SMRP 濃度の参考基準値を 1.5 nmol/L とした場合，この値よりも高値を示す症例の割合（陽性率）は，それぞれ MM66%（56/85 例），肺癌 21%（51/240 例），石綿非関連良性疾患 18%（24/136 例），石綿関連良性疾患 15%（24/157 例），高血圧・慢性心疾患 9%（7/74 例）であった。MM における血清 SMRP 濃度は，比較対照群および健常者に比較して有意に高値であった。MM の原発部位別の陽性率は，胸膜 65%（50/77 例），腹膜 86%（6/7 例）であった。

3．MPM 各病期における血清 SMRP 濃度および陽性率（図 2，表 2）

病期が確定した MPM69 例について，各病期における血清 SMRP 濃度および陽性率を検討した結果，各病期間での血清 SMRP 濃度に有意差はなく，陽性率は，それぞれ I 期 64%（7/

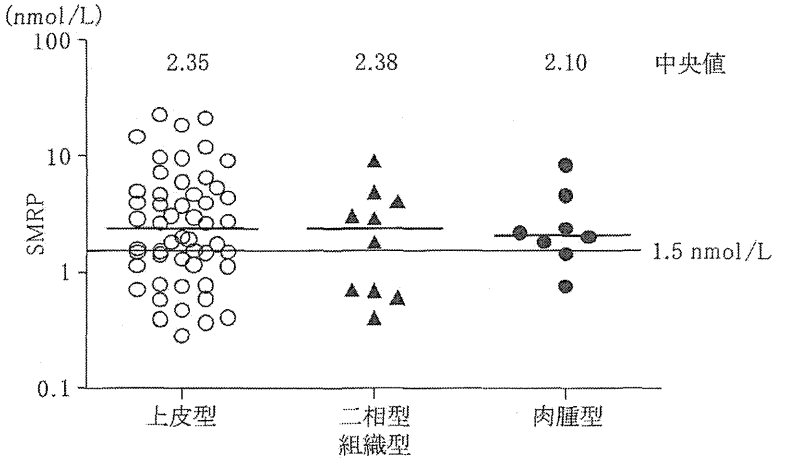

図 3　悪性胸膜中皮腫の各組織型における血清 SMRP 濃度の分布

表 3　悪性胸膜中皮腫の各組織型における血清 SMRP 濃度および陽性率

	上皮型	二相型	肉腫型
症例総数	52	10	8
中央値（nmol/L）	2.35	2.38	2.10
SD（nmol/L）	5.19	2.72	2.48
陽性数	34	6	6
陽性率	65%	60%	75%

SD：standard deviation

11例），II期67%（8/12例），III期55%（6/11例），IV期69%（24/35例）であった。

4．MPM各組織型における血清SMRP濃度および陽性率（図3，表3）

組織型の確定し得たMPM70例の内訳は，上皮型52例，二相型10例，肉腫型8例であった。各組織型間における血清SMRP濃度に有意差はなく，陽性率は，それぞれ上皮型65%（34/52例），二相型60%（6/10例），肉腫型75%（6/8例）であった。

IV．考　　察

近年，SMRPを認識する2種類のモノクローナル抗体（OV569と4H3）を用いた新しい定量的ELISAキットであるMESOMARK™の開発によって，血清SMRP濃度の測定が可能となった[8)~16)]。これらの報告では，血清SMRP濃度は健常者および石綿曝露者，石綿関連良性胸膜疾患，肺癌などの対照疾患に比較して，MMにおいて有意に上昇していた[8)~16)]。MESOMARK™と同一の抗体を使用したCLEIAキットであるルミパルス® メソテリンを用いた本試験においても，血清SMRP濃度は，健常者および肺癌，良性呼吸器疾患，高血圧・慢性心疾患に比較してMMにおいて有意に上昇していた。この結果は，MM血清診断におけるSMRPの高い診断性能と測定結果の普遍性および再現性とを意味するものと考えられた。これまでのMESOMARK™を用いた測定報告では，MMにおける血清SMRP濃度中央値は0.79から2.39 nmol/Lの範囲に分布していた[8)~16)]。本試験におけるMMの血清SMRP

濃度中央値も2.38 nmol/Lであり，この範囲内に含まれていた。参考基準値（カットオフ値）に関しては，健常者を対象とした結果から，MESOMARK™およびルミパルス® メソテリンともに，1.5 nmol/Lに設定されている[9)17)]。本試験において，健常者110名のうち99%が，血清SMRP濃度1.5 nmol/L（参考基準値）未満であった。この参考基準値の条件下で，MMにおけるSMRPの陽性率（感度）は66%であった。一方，これまでのMESOMARK™を用いた測定報告では，SMRPの感度は48%から80%（中央値68.2%）と報告されており，ルミパルス® メソテリンの感度もこれらの測定報告に匹敵するものと考えられる。

MPMにおけるSMRP陽性率は65%であり，腹膜中皮腫を含むMM全症例の陽性率と概ね同等であった。MPM各病期間での血清SMRP濃度と陽性率に有意差はなく，I-II期においても，III-IV期に匹敵する陽性率が得られた。このことは，本キットが高感度の測定系であることから，早期例においても血清SMRPの検出が可能であることが推察された。Passら[13)]，II期以上の症例はI期症例に比較して血清SMRP濃度が有意に上昇することを報告しているが，その他の報告では病期と血清SMRP濃度との明らかな関連性は指摘されなかった[9)10)14)]。今後，MPM早期診断マーカーとしてのSMRPの意義を明らかにするために，早期例を中心とした検討が必要になるものと考える。

MPMの各組織型と血清SMRP濃度との関連性に関して，本試験では，各組織型間での血清SMRP濃度と陽性率に有意差はなく，上皮型のみならず肉腫型においても75%が陽性を示した。これまでのMESOMARK™を用いた測定報告では，組織型と血清SMRP濃度との関連性については一定の見解が得られておらず，上皮型が肉腫型に比較して有意に高値であるという報告[7)8)10)15)]と，本試験と同様，各組織型間で有意差はないとする報告[9)11)13)14)]とに分かれている。

MMの診断には，石綿曝露歴，臨床症状，血液生化学検査，画像および内視鏡検査，体腔液細胞診，生検病理組織診などを駆使した総合的なアプローチが必要とされる[4)]。しかしながら，高齢者や全身状態不良例では，侵襲的検査の適応外となることも多く，診断に苦慮する場合も少なくない。このような症例では，MMに対して診断性能の高いバイオマーカーによる血清診断が重要な役割を担う。ルミパルス® メソテリンによる血清SMRP濃度測定は，一般の血液検査と同様，患者から採取した血清または血漿を用いて全自動分析装置にて約30分間で測定が完了する。したがって，患者への侵襲もなく，技術的にも容易に短時間で測定結果を得ることが可能であることから，今後，本キットは，MMを疑う患者に対して汎用されていくことが予想される。また，MM発症リスクの高い石綿曝露者を対象とした血液スクリーニング検査のひとつとして用いられることも想定される。

おわりに

現状では，石綿曝露者に発症した胸水貯留が良性石綿胸水であるのか，MPMの初期症状であるのかを鑑別することは困難である。しかし，この時期での診断機会を逸することは早期MPMの発見を見逃すこととなる。今回の検討では，SMRP測定がMPMの早期診断に有用なバイオマーカーとなることを示唆する結果が得られており，今後のさらなる研究の成果に期待が寄せられる。

文　献

1) 中野孝司．悪性胸膜中皮腫．呼吸 **28**：509-515, 2009.
2) 中野孝司．悪性胸膜中皮腫（びまん性悪性胸膜中皮腫）．別冊日本臨牀 呼吸器症候群（第2版）**10**：380-384, 2009.
3) Tsao AS, Wistuba I, Roth JA, Kindler HL：Malignant pleural mesothelioma. J Clin Oncol **27**：2081-2090, 2009.
4) 福岡和也，田中文啓，辻村　亨，玉置知子，長谷

川誠紀，中野孝司：中皮腫に対する早期診断指標の探索的研究．日衛誌（Jpn. J. Hyg.）**66**：553-557, 2011.

5) Scholler N, Fu N, Yang Y, Ye Z, Goodman GE, Hellstrom KE, Hellstrom I：Soluble member (s) of the mesothelin/megakaryocyte potentiating factor family are detectable in sera from patients with ovarian carcinoma. Proc Natl Acad Sci USA **96**：11531-11536, 1999.
6) Hassan R, Bera T, Pasten I：Mesothelin：a new target for immunotherapy. Clin Cancer Res **10**：3937-3942, 2004.
7) Robinson BWS, Creaney J, Lake R, Nowak A, Musk AW, Klerk ND, Winzell P, Hellstrom KE, Hellstrom I：Mesothelin-family proteins and diagnosis of mesothelioma. Lancet **362**：1612-1616, 2003.
8) Scherpereel A, Grigorlu B, Conti M, Gey T, Gregoire M, Copin MC, Devos P, Chahine B, Porte H, Lassalle P：Soluble mesothelin-related peptides in the diagnosis of malignant pleural mesothelioma. Am J Respir Crit Care Med **173**：1155-1160, 2006.
9) Beyer HL, Geschwindt RD, Glover CL, Tran L, Hellstrom I, Hellstrom KE, Miller MC, Verch T, Allard WJ, Pass HI, Sardesai NY：Mesomark：a potential test for malignant pleural mesothelioma. Clin Chem **53**：666-672, 2007.
10) Cristaudo A, Foddis R, Vivaldi A, Guglielmi G, Dipalma N, Filiberti R, Neri M, Ceppi M, Paganuzzi M, Ivaldi GP, Mencoboni M, Canessa PA, Ambrosino N, Chella A, Mutti L, Puntoni R：Clinical significance of serum mesothelin in patients with mesothelioma and lung cancer. Clin Cancer Res **13**：5076-5081, 2007.
11) Creaney J, Van Bruggen I, Hof M, Segal A, Musk AW, de Klerk N, Horick N, Skates SJ, Robinson BW：Combined CA 125 and mesothelin levels for the diagnosis of malignant mesothelioma. Chest **132**：1239-1246, 2007.
12) Amati M, Tomasetti M, Scartozzi M, Mariott L, Alleva R, Pignotti E, Borghi B, Valentino M, Governa M, Neuzil J, Santarelli L：Profiling tumor-associated markers for early detection of malignant mesothelioma：an epidemiologic study. Cancer Epidemiol Biomarkers Prev **17**：163-170, 2008.
13) Pass HI, Wali A, Tang N, Ivanova A, Ivanov S, Harbut M, Carbone M, Allard J：Soluble mesothelin-related peptide level elevation in mesothelioma serum and pleural effusions. Ann Thorac Surg **85**：265-272, 2008.
14) Schneider J, Hoffmann H, Dienemann H, Herth FJF, Meister M, Muley T：Diagnostic and prognostic value of soluble mesothelin-related proteins in patients with malignant pleural mesothelioma in comparison with benign asbestosis and lung cancer. J Thorac Oncol **3**：1317-1324, 2008.
15) Creaney J, Yeoman D, Demelker Y, Segal A, Musk AW, Skates SJ, Robinson BWS：Comparison of osteopontin, megakaryocyte potentiating factor, and mesothelin proteins as markers in the serum of patients with malignant mesothelioma. J Thorac Oncol **3**：851-857, 2008.
16) Portal JAR, Becerra ER, Rodriguez DR, Michavila IA, Martinez AQ, Roza CD, Jimenez AL, Montes II, Rivas PC：Serum levels of soluble mesothelin-related peptides in malignant and nonmalignant asbestos-related pleural disease：Relation with past asbestos exposure. Cancer Epidemiol Biomarkers Prev **18**：646-650, 2009.
17) 中町　衛，桑原明子，村上　弘，皆川英孝，森山和重：ルミパルス　メソテリンの基礎性能評価．医学と薬学 **65**：261-267, 2011.

*　　*　　*

A homozygous nonsense mutation in the gene for *Tmem79*, a component for the lamellar granule secretory system, produces spontaneous eczema in an experimental model of atopic dermatitis

Takashi Sasaki, PhD,[a,b]* Aiko Shiohama, PhD,[c,d]* Akiharu Kubo, MD, PhD,[a,b] Hiroshi Kawasaki, MD, PhD,[a] Akemi Ishida-Yamamoto, MD, PhD,[e] Taketo Yamada, MD, PhD,[f] Takayuki Hachiya, PhD,[g] Atsushi Shimizu, PhD,[h] Hideyuki Okano, MD, PhD,[i] Jun Kudoh, PhD,[d] and Masayuki Amagai, MD, PhD[a,c] *Tokyo, Asahikawa, and Nagano, Japan*

Background: Flaky tail *(ma/ma $Flg^{ft/ft}$)* mice have a frameshift mutation in the filaggrin *(Flg^{ft})* gene and are widely used as a model of human atopic dermatitis associated with *FLG* mutations. These mice possess another recessive hair mutation, *matted (ma)*, and develop spontaneous dermatitis under specific pathogen-free conditions, whereas genetically engineered $Flg^{-/-}$ mice do not.

Objective: We identified and characterized the gene responsible for the matted hair and dermatitis phenotype in flaky tail mice.

Methods: We narrowed down the responsible region by backcrossing *ma/ma* mice with wild-type mice and identified the mutation using next-generation DNA sequencing. We attempted to rescue the matted phenotype by introducing the wild-type *matted* transgene. We characterized the responsible gene product by using whole-mount immunostaining of epidermal sheets.

Results: We demonstrated that *ma*, but not Flg^{ft}, was responsible for the dermatitis phenotype and corresponded to a *Tmem79* gene nonsense mutation (c.840C>G, p.Y280*), which encoded a 5-transmembrane protein. Exogenous *Tmem79* expression rescued the matted hair and dermatitis phenotype of $Tmem79^{ma/ma}$ mice. Tmem79 was mainly expressed in the *trans*-Golgi network in stratum granulosum cells in the epidermis in both mice and humans. The $Tmem79^{ma/ma}$ mutation impaired the lamellar granule secretory system, which resulted in altered stratum corneum formation and a subsequent spontaneous dermatitis phenotype.

Conclusions: The $Tmem79^{ma/ma}$ mutation is responsible for the spontaneous dermatitis phenotype in *matted* mice, probably as a result of impaired lamellar granule secretory system and altered stratum corneum barrier function. (J Allergy Clin Immunol 2013;132:1111-20.)

Key words: *Atopic dermatitis, skin barrier, stratum corneum, trans-Golgi network, filaggrin*

Loss-of-function mutations in the filaggrin *(FLG)* gene cause ichthyosis vulgaris, a common autosomal dominant keratinization disorder characterized by scaly skin, and are a major factor predisposing one to atopic disorders, including atopic dermatitis (AD), atopic asthma, hay fever, and food allergy.[1-6] Filaggrin is a major component of the stratum corneum (SC) and plays an important role in its structural integrity.[7] Consequently, defects in the *FLG* mutation–associated SC barrier lead to increased percutaneous allergen exposure and a subsequent heightened immune reaction.[8,9] *FLG* mutations exist in 15% to 55% of patients with AD of various ethnic groups.[4,10] Other predisposing factors remain to be identified in the remaining 45% to 85% of patients with AD.

The flaky tail *(Flg^{ft})* mouse phenotype first arose as a spontaneous recessive mutation in 1958 on the background of the existing recessive hair phenotype, matted *(ma)*. Since then, the mice have been maintained as a mixed strain because these loci are closely linked on mouse chromosome 3.[11,12] The *ma/ma $Flg^{ft/ft}$* mice express a truncated profilaggrin (approximately 215 kDa) instead of the normal profilaggrin (>500 kDa) because of a 1-bp deletion mutation, c.5303delA, which leads to premature termination 154 codons downstream (p.Asn1768Thrfs*154) in the murine *Flg* gene.[13,14] Therefore *ma/ma $Flg^{ft/ft}$* mice are widely used as a model of AD to investigate its pathophysiologic mechanisms.[15-20] The *ma/ma $Flg^{ft/ft}$* mice have enhanced percutaneous allergen priming and develop spontaneous dermatitis under specific pathogen-free (SPF) conditions.[14] In contrast, genetically engineered $Flg^{-/-}$ mice have altered SC barrier function and enhanced percutaneous allergen priming but do not develop spontaneous dermatitis under SPF conditions.[8]

From the Departments of [a]Dermatology, [f]Pathology, [h]Molecular Biology, and [i]Physiology, [b]the Center for Integrated Medical Research, [c]the MSD Endowed Program for Allergy Research, and [d]the Laboratory of Gene Medicine, Keio University School of Medicine, Tokyo; [e]the Department of Dermatology, Asahikawa Medical University; and [g]Medical and Biological Laboratories Co Ltd, Nagano.

*These authors contributed equally to this work.

M.A. and J.K. are supported by Health Labour Sciences Research Grant for Research on Allergic Disease and Immunology from the Ministry of Health, Labour, and Welfare of Japan. A.K., A.I.-Y., and A.S. are supported by Grants-in-Aid for Scientific Research from the Ministry of Education, Culture, Sports, Science, and Technology of Japan. M.A, H.O., J.K., A.S., and T.S. are supported by the Global Centre of Excellence (GCOE) program at Keio University from the Ministry of Education, Culture, Sports, Science, and Technology of Japan.

Disclosure of potential conflict of interest: M. Amagai has been supported by one or more grants from a government granting agency; has consultancy arrangements with Daiichi Sankyo Co, Novartis Pharma K.K., and GlaxoSmithKline K.K.; and has received one or more grants from or has one or more grants pending with MSD K.K. and Maruho Co Ltd. A. Shiohama, A. Kubo, and J. Kudoh have been supported by one or more grants from a government granting agency. H. Okano has been supported by one or more grants from a government granting agency and has consultancy arrangements with San Bio, Eisai Co Ltd, and Daiichi Sankyo Co Ltd.

Received for publication June 28, 2013; revised August 8, 2013; accepted for publication August 8, 2013.

Available online September 20, 2013.

Corresponding author: Masayuki Amagai, MD, PhD, Department of Dermatology, Keio University School of Medicine, 35 Shinanomachi, Shinjyuku-ku, Tokyo, Japan. E-mail: amagai@med.keio.ac.jp.

0091-6749/$36.00

http://dx.doi.org/10.1016/j.jaci.2013.08.027

Abbreviations used
AD: Atopic dermatitis
CDSN: Corneodesmosin
Flg: Filaggrin
LG: Lamellar granule
ma: Matted
SC: Stratum corneum
SG: Stratum granulosum
SNV: Single nucleotide variation
SPF: Specific pathogen free
TEWL: Transepidermal water loss
TGN: *Trans*-Golgi network
WT: Wild type

To examine this conflicting finding, we segregated the *ma* and Flg^{ft} mutations by backcrossing with wild-type (WT) mice (C57BL/6) to generate congenic strains and demonstrated that *ma*, but not Flg^{ft}, is responsible for the dermatitis phenotype and corresponds to a nonsense mutation (c.840C>G, p.Y280*) in the *Tmem79* gene. We further characterized the epidermal expression pattern of Tmem79 in addition to the effects on lamellar granule (LG) secretion and SC formation caused by the mutation.

METHODS

Mice

Flaky tail mice (*ma/ma* $Flg^{ft/ft}$) were obtained from Jackson Laboratory (Bar Harbor, Me). Flaky tail mice were backcrossed with C57BL/6J mice (CLEA Japan, Tokyo, Japan) to generate *ma/ma* and $Flg^{ft/ft}$ mice. We genotyped Flg^{ft}, as described previously.[14]

Biophysical skin measurements

Skin hydration was evaluated by analyzing the skin electrical impedance with a Corneometer ASA-M2 (Asahi Biomed, Yokohama, Japan). Transepidermal water loss (TEWL) was measured with a VAPOSCAN AS-VT100RS (Asahi Biomed). All data are the median of 3 recordings.

DNA sequencing and transmembrane topology analysis

To narrow the *ma* candidate region, we established 9 markers that distinguished between C57BL/6 and CBA mouse alleles based on single nucleotide polymorphisms (SNPs). Genomic DNAs from $Tmem79^{ma/ma}$, CBA, and C57BL/6 mice were sequenced by means of targeted resequencing with the Next Generation DNA Sequencer. Briefly, the extracted genomic DNA was enriched with the SureSelect Target Enrichment System (Agilent Technologies, Tokyo, Japan) and sequenced with the Illumina Genome Analyzer II (Illumina, Tokyo, Japan). The DNA sequence reads were mapped to the mouse reference genome (mm19) by using bwa,[21] and single nucleotide variations (SNVs)/indels were extracted with SAMtools[22] (see the Methods section in this article's Online Repository at www.jacionline.org for details). SOSUI (http://bp.nuap.nagoya-u.ac.jp/sosui/) and Octopus (http://octopus.cbr.su.se/) were used to predict the transmembrane location and topology.[23,24]

Construction of a *Tmem79* transgenic vector and generation of $Tmem79^{Tg}$ mice

The 9223-bp genomic region, including the entire *Tmem79* gene on bacterial artificial chromosome DNA RP23-168E1, was subcloned into pUC118 vector by using the Red/ET recombination system (GeneBridges, Heidelberg, Germany; see Fig E1 in this article's Online Repository at www.jacionline.org) to generate $Tmem79^{Tg}$ mice. The linearized *Tmem79* transgenic vector was injected into pronuclei of fertilized eggs and implanted into pseudopregnant females. The mouse transgene was screened by using PCR to amplify the boundary region between the pUC118 vector and the *Tmem79* genomic sequence.

Evaluation of dermatitis severity

Mouse behavior was videotaped, and the number of scratches within a 5-minute period was recorded 3 times; the median value was analyzed. We scored the total clinical skin severity of the mice from 0 to 3 for 5 skin-associated phenotypes (pruritus, erythema, edema, excoriation, and scaling), as previously described.[25] The total serum IgE level was measured with an ELISA kit (Bethyl Laboratories, Montgomery, Tex).

Whole-mount immunostaining of epidermal sheets

Epidermal sheets from mouse ear and human shoulder skin were immunostained for Tmem79 and other marker proteins. The skin specimens were treated with 3.8% ammonium thiocyanate, and the dermis and epidermis were separated. Whole-mount staining of epidermal sheets was performed, as described previously.[26] Tmem79 and other organelle marker proteins were observed by using z-stack scanning with a Leica TCS SP5 confocal microscope (Leica Microsystems, Tokyo, Japan).

Antibodies

Rabbit antibodies were raised against synthetic peptides containing Tmem79 N-terminal residues 99 to 115 (Ab^{matN}) and C-terminal residues 376 to 391 (Ab^{matC}). Other antibodies used in this study are shown in the Methods section in this article's Online Repository.

Immunoelectron microscopy

Postembedding immunoelectron microscopy was performed, as described previously, with slight modification.[27] Anti-TMM79 rabbit antibody (Abgent, San Diego, Calif) and anti-human *trans*-Golgi network (TGN) 46 sheep antibody (AbD Serotec, Oxford, United Kingdom) were used as primary antibodies, and 10-nm gold-labeled donkey anti-sheep IgG (BBInternational, Cardiff, United Kingdom) and 5-nm gold-labeled goat anti-rabbit IgG (BBInternational) were used as secondary antibodies.

Tape stripping

The dorsal skin of P5 neonatal mice was repeatedly tape stripped at the same sites with Cryofilm Type 2C (Leica Microsystems) to assess SC layer detachment under mechanical stress. The remaining SC layer was evaluated by using safranin staining, and the number of focal abnormal desquamated regions in which all layers peeled off were counted.

Statistical analysis

All experiments were analyzed by using 2-tailed Student *t* tests with GraphPad Prism 5.0 (GraphPad Software, San Diego, Calif). All results are presented as means and SEMs. A P value of less than .05 was considered to indicate statistical significance.

RESULTS

Matted mutation, but not filaggrin mutation, is responsible for the matted hair and spontaneous dermatitis phenotype

To generate each congenic mouse strain (*ma/ma* and $Flg^{ft/ft}$), we segregated the *ma* and Flg^{ft} mutations by backcrossing with WT mice (C57BL/6). As a result, *ma/ma* mutant mice, which displayed the *matted* hair phenotype, developed spontaneous

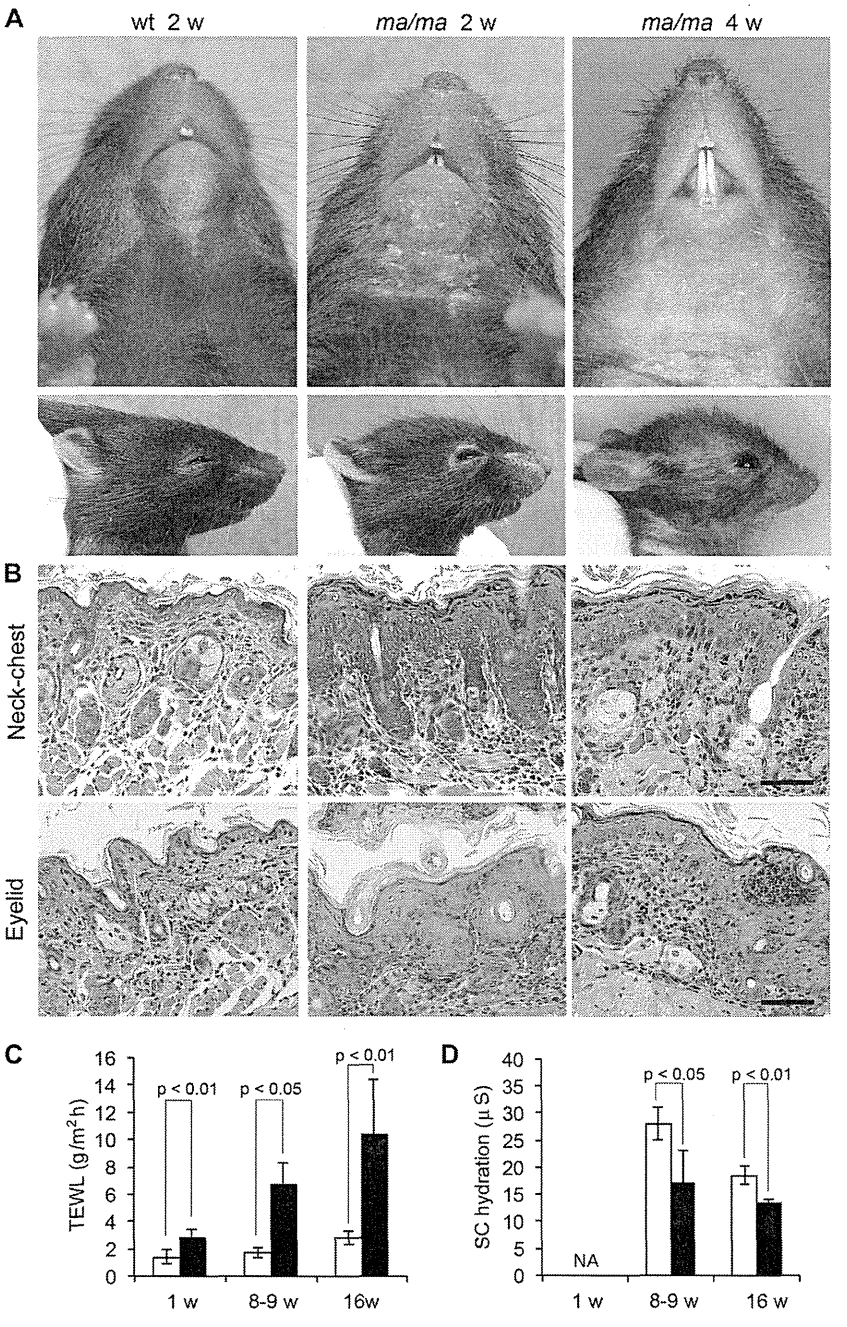

FIG 1. Development of spontaneous dermatitis in *ma/ma* mice. **A,** Gross phenotype of 2-week-old WT (C57BL/6), 2-week-old *ma/ma*, and 4-week-old *ma/ma* mice. **B,** Histology of the skin on the neck-chest area and eyelid. *Bars* = 100 μm. **C** and **D,** TEWL and SC hydration of the skin on the neck-chest area of 1-, 8-, and 16-week-old WT (C57BL/6: *white bars*, n = 5) and *ma/ma* (*black bars*, n = 5) mice. *NA*, Not analyzed.

dermatitis with scratching behavior, whereas $Flg^{ft/ft}$ mice did not have dermatitis under SPF conditions (Fig 1, *A* and *B*, and see Table E1 in this article's Online Repository at www.jacionline.org). TEWL was higher and SC hydration was lower in *ma/ma* mice compared with WT mice (Fig 1, *C* and *D*). The enhanced TEWL and histologic changes, such as acanthosis with leukocyte infiltration, were observed as early as 1 week, when no apparent scratching behavior was observed, indicating that there is a primary defect in the skin leading to the development of dermatitis in *ma/ma* mice. Therefore we concluded that *ma*, but not Flg^{ft} or Flg^{-}, is responsible for the development of spontaneous dermatitis in *ma/ma* $Flg^{ft/ft}$ mice.

Identification of the gene responsible for the spontaneous dermatitis phenotype in *ma/ma* mice

Next we sought to identify the genetic mechanism underlying the *ma* mutant and study the detailed function of the responsible gene product. The *ma* locus is located between *spa (Glrb)* and *ft (Flg)* in an 80.7- to 93.1-Mb region of mouse chromosome 3.[12]